

Using CMBR analysis tools for flow anisotropies in relativistic heavy-ion collisions

Ananta P. Mishra,* Ranjita K. Mohapatra,† P. S. Saumia,‡ and Ajit M. Srivastava§
Institute of Physics, Sachivalaya Marg, Bhubaneswar 751005, India

Recently we have shown that there are crucial similarities in the physics of cosmic microwave background radiation (CMBR) anisotropies and the flow anisotropies in relativistic heavy-ion collision experiments (RHICE). We also argued that, following CMBR anisotropy analysis, a plot of root-mean square values of the flow coefficients, calculated in a lab fixed frame for RHICE, can yield important information about the nature of initial state anisotropies and their evolution. Here we demonstrate the strength of this technique by showing that elliptic flow for non-central collisions can be directly determined from such a plot without any need for the determination of event-plane.

I. INTRODUCTION

Relativistic heavy-ion collision experiments (RHICE) are often termed as *Little Bangs* in analogy of the *Big Bang* representing the initial stage of the Universe. Indeed, there are tempting similarities between the early universe and these experiments. For example, it is often mentioned that the surface of last scattering for the cosmic microwave background radiation (CMBR) is similar to the freezeout surface in RHICE in the sense that one has to learn about the early stages of the system from hadrons coming out from the freezeout surface, just as CMBR encodes information about the early universe. However, these correspondences and analogies have been primarily made from a motivational view point. It has recently been shown by us [1] that the physics of RHICE may have deeper connections, not just with the above mentioned aspects of CMBR, but even to the most celebrated aspect of inflationary physics of the universe namely the presence of superhorizon fluctuations.

Following the techniques used for CMBR anisotropy analysis, it was proposed in ref.[1] that instead of focusing on the average values of the flow coefficients v_n , one should calculate root-mean square values of the flow coefficients v_n^{rms} . Further, these calculations should be performed in a lab fixed frame, which eliminates the difficulties associated with determination of event plane for conventional elliptic flow analysis for non-central collisions. To distinguish from the conventional flow coefficients v_n which are defined with respect to the event plane, we will denote, in this paper, the flow coefficients defined with respect to the lab fixed frame as \tilde{v}_n . The root mean square value is then denoted as \tilde{v}_n^{rms} . Plots of \tilde{v}_n^{rms} (denoted as v_n^{rms} in [1]) using model estimates based on initial energy density anisotropies from HIJING [2] were given there for large range of values of n (with n ranging from 1 to 30) for central collisions and it was argued that such plots can yield important information about the nature of initial state anisotropies and their evolution for RHICE.

In this paper we demonstrate the strength of this analysis technique by showing that a plot of values of \tilde{v}_n^{rms} vs. n can be used for directly probing various flow coefficients, in particular, the elliptic flow for non-central collisions [3], without any need for the determination of event-plane. For non-central collisions, a plot of \tilde{v}_n^{rms} (using model estimates from the spatial distribution of initial parton energy density), shows a prominent peak at $n = 2$, as we will see below. Further, the height of the peak increases with increasing value of the impact parameter b , thus allowing direct determination of elliptic flow (in terms of \tilde{v}_2^{rms}). This can be very useful for analyzing huge wealth of data as the determination of event plane for each event becomes redundant.

The correspondence between the CMBR physics and RHICE explored at a deeper level as discussed in [1] may lead to new set of interesting phenomena and new techniques for RHICE. We mention that such a connection between physics of RHICE and that of inflationary universe was never anticipated earlier, and indeed, at first sight, it looks surprising that a concept like superhorizon fluctuation which arises from highly non-trivial, superluminal expansion phase of the very early universe could have any relevance for relativistic heavy-ion collision experiments in laboratory. Such superhorizon fluctuations in RHICE originate from the fact that in the center of mass frame the thermalization happens rather quickly, within about 1 fm. This time is too short for any fluctuations (inhomogeneities) in the transverse direction to disappear, by processes of homogenization, which have wavelengths larger than 1 fm. Initial parton energy density distribution from HIJING show that transverse fluctuations with wavelengths significantly

*Electronic address: apmishra@iopb.res.in

†Electronic address: ranjita@iopb.res.in

‡Electronic address: saumia@iopb.res.in

§Electronic address: ajit@iopb.res.in

larger than 1 fm are necessarily present at the time 1 fm even in central collisions. These arise from localization of partons inside initial nucleons, as well as from the fluctuations in nucleon coordinates. Analyzing the development of flow from such initial large wavelength fluctuations, we had argued that the anisotropies in the final particle momenta may show characteristic features of acoustic oscillations of subhorizon modes as well as suppression of modes which remain superhorizon at the freezeout stage. We will show below that such features do not mask the peak at $n = 2$ in non-central collisions.

The paper is organized in the following manner. In section II, we recall the adoption of CMBR anisotropy analysis method for the case of RHICE. Here we also show that calculations of \tilde{v}_n^{rms} in the lab fixed frame can directly yield information about various flow coefficients defined with respect to the event plane. In particular, the conventional elliptic flow can be determined in this manner. Section III presents the results of the application of these analysis methods for the determination of \tilde{v}_n^{rms} for the case of non-central collisions. In section IV we discuss the p_T dependence, and in section V we discuss the issue of anisotropic detector acceptance. Section VI presents conclusions and discussions.

II. USING CMBR ANALYSIS TOOLS FOR RHICE

Traditional analysis of elliptic flow in RHICE [3] is based on measuring the average value of the 2nd Fourier coefficient of particle transverse momentum anisotropy. The average value is determined by carrying out the Fourier expansion in the event-plane reference frame. Even for the so-called 'central collisions' one determines event plane for very small impact parameter collisions and then carries out the traditional analysis of determination of average flow [4]. However, determination of event plane is highly non-trivial making determination of higher flow coefficients very difficult. Indeed, flow coefficients have been determined only upto v_6 .

It is here that the use of techniques of CMBR analysis can make a significant difference. For CMBR, the temperature anisotropies are analyzed using spherical harmonics, as appropriate for the surface of 2-sphere (the CMBR sky) [5]. The coefficients of the expansion (denoted as a_{lm} corresponding to the spherical harmonic Y_{lm}) are degenerate in the argument m and when averaged over different values of m yield zero averages due to isotropy of the universe (when suitably corrected for local velocities etc.). What one plots is the variance of a_{lm} denoted by C_l and this leads to the celebrated power spectrum of CMBR anisotropies [5].

We propose using the same technique [1] for analyzing particle momentum anisotropies, using lab fixed frame, in RHICE to probe the generation and evolution of flow. For RHICE, focusing on central rapidity region, one will be analyzing momentum anisotropies on a circle, requiring use of the Fourier coefficients, which we denote as \tilde{v}_n to distinguish from the conventional flow coefficients v_n which are defined with respect to the event plane. With a fixed lab frame, the event average values of these \tilde{v}_n s will all be zero due to rotational symmetry. We then propose to use the variance of \tilde{v}_n , i.e. \tilde{v}_n^{rms} in analogy with C_l for CMBR.

We first establish the relation between \tilde{v}_n^{rms} calculated in the lab fixed frame and the conventional flow coefficients v_n which are defined with respect to the event plane as follows

$$\rho(\phi') = \sum_{n=-\infty}^{\infty} v_n e^{in\phi'} \quad (1)$$

Where the angle ϕ' is measured with respect to the event plane. Assuming that the event plane is oriented by angle ψ with respect to the lab fixed frame, we can write the above equation in the lab fixed frame as,

$$\rho_\psi(\phi) = \sum_{n=-\infty}^{\infty} v_n e^{in(\phi-\psi)} \quad (2)$$

where now the angle ϕ is measured with respect to the lab fixed frame. The subscript for $\rho_\psi(\phi)$ remind us that the above Fourier series expansion uses the flow coefficients defined with respect to the event plane which is oriented at an angle ψ in the lab frame. Without the knowledge of ψ , we will calculate the lab fixed flow coefficients $\tilde{v}_n(\psi)$ as

$$\tilde{v}_n(\psi) = \frac{1}{2\pi} \int_{-\pi}^{\pi} \rho_\psi(\phi) e^{-in\phi} d\phi \quad (3)$$

Here the argument ψ in $\tilde{v}_n(\psi)$ is used to remind that these quantities are calculated in the lab fixed frame, and are different from the values of conventional flow coefficients v_n defined in Eq.(1). The event average value $\overline{\tilde{v}_n}$ of these

flow coefficients \tilde{v}_n , is obtained by averaging \tilde{v}_n over a large number of events (of similar type, e.g. centrality etc.). $\overline{\tilde{v}_n}$ is determined by the following expression

$$\overline{\tilde{v}_n} = \frac{1}{2\pi} \int_{-\pi}^{\pi} \left(\frac{1}{2\pi} \int_{-\pi}^{\pi} \rho_{\psi}(\phi) e^{-in\phi} d\phi \right) d\psi \quad (4)$$

Integration over ψ reflects the random variation of the orientation of the event plane in the lab fixed frame from event to event. By changing the order of integration for $d\phi$ and $d\psi$, and using Eq.(2), we immediately see that the $\overline{\tilde{v}_n} = 0$ for all $n > 0$ as mentioned above.

We next calculate the event averaged values of $|\tilde{v}_n(\psi)|^2$ as

$$(\tilde{v}_n^{rms})^2 = \overline{\tilde{v}_n^2} = \frac{1}{2\pi} \int_{-\pi}^{\pi} d\psi \tilde{v}_n(\psi) \tilde{v}_n^*(\psi) \quad (5)$$

Straightforward calculation using Eqs.(2)-(5) gives

$$\tilde{v}_n^{rms} = |v_n| \quad (6)$$

This is an important result. It shows that various conventional flow coefficients v_n , defined with respect to the event plane, can be directly calculated in the lab fixed frame in terms of \tilde{v}_n^{rms} . However, one has to be careful in interpreting the above equation. The above equation has been derived for the event averaged values. Thus the right hand side $|v_n|^2$ also represents the event averaged value of the conventional flow coefficients. Even if we assume that each event is almost identical in terms of centrality selection etc. (which it is not), still there will be random fluctuations in the fluid especially due to initial state fluctuations [1]. If the contributions of such fluctuations becomes dominant then the right hand side of the above equation will not have a neat interpretation of relating to $|v_n|$ defined with respect to the event plane.

Fortunately this problem does not exist for the elliptic flow v_2 . Below we will see, with model calculations of \tilde{v}_2^{rms} for non-central events from HIJING, that the contribution arising from the elliptic shape of the produced partons in the overlap region is very large compared to the contribution from the random, initial state fluctuations. This will be seen as a prominent peak in the plot of \tilde{v}_n^{rms} vs. n at $n = 2$. Thus, as far as determination of the elliptic flow is concerned, Eq.(6) shows that calculation of \tilde{v}_2^{rms} in the lab fixed frame can be used to determine the value of $|v_2|$. Neglecting the contributions of random fluctuations, symmetry of the elliptical shape of the overlap region for non-central collisions will then imply that $|v_2|$ is the same as v_2 conventionally defined as the coefficient of the $\cos 2\phi$ term.

For other values of n the Eq.(6) has to be suitably interpreted with proper account of event by event random fluctuations. As we have emphasized, values of \tilde{v}_n^{rms} determined by averaging over events should be directly used to probe the statistical properties of fluctuations and anisotropies of the initial plasma region (as is done for CMBR). Hydrodynamical simulations, with proper incorporation of such fluctuations can then be used to predict the values of \tilde{v}_n^{rms} whose comparison with data can then be used to constrain/determine various physical inputs such as equation of state, viscosity etc.

We now describe our method for calculating \tilde{v}_n^{rms} using HIJING [6]. We first recall from ref. [1] the estimates of initial spatial anisotropies. We start with the initial transverse energy density distribution for Au-Au collision at 200 GeV/A center of mass energy from HIJING. For parton positions we use random locations inside the parent nucleon, (similarly, for partons produced from the string systems, random position are used along the line joining the two corresponding nucleons). The transverse energy density at a given transverse position \vec{x} , at proper time $\tau = \tau_{eq}$, is taken as [2],

$$\epsilon_{tr}(\vec{x}, \tau_{eq}) = \frac{1}{\Delta A} \sum_i E_{tr}^i F(\tau_{eq}, p_{tr}) \delta^2(\vec{x} - \vec{x}_0^i - \vec{v}^i \tau_{eq}) \Delta(y^i) \quad (7)$$

where \vec{x}_0^i denotes the initial transverse coordinates of the i_{th} parton (determined using the coordinates of the parent nucleon in HIJING as discussed above), E_{tr}^i is its transverse energy, p_{tr} the transverse momentum, and \vec{v}^i is its transverse velocity. For the rapidity window we take $\Delta(y^i) = 1$ centered at $y = 0$, [2]. The sum over i includes all partons in a small transverse area element $\Delta A (\simeq 0.5 \text{ fm}^2)$ at position \vec{x} . We have included a factor $F(\tau_{eq}, p_{tr}) \equiv 1/(1 + 1/(p_{tr}\tau_{eq})^2)$ to account for the probability of formation of partons with zero rapidity [2].

We assume that the hydrodynamic description becomes applicable by $\tau = \tau_{eq}$, which we take to be 1 fm and calculate the anisotropies in the fluctuations in the spatial extent $R(\phi)$ at this stage, where $R(\phi)$ represents ϵ_{tr} weighted average of the transverse radial coordinate in the angular bin at azimuthal coordinate ϕ [1]. As emphasized above, angle ϕ is taken in a lab fixed coordinate frame. We divide the region in 50 - 100 bins of azimuthal angle ϕ , and calculate the Fourier coefficients of the anisotropies in $\delta R/R \equiv (R(\phi) - \bar{R})/\bar{R}$ where \bar{R} is the angular average of $R(\phi)$. Note that in this way we are representing all fluctuations essentially in terms of fluctuations in the boundary of the initial region. We use F_n to denote Fourier coefficients for these spatial anisotropies, and use \tilde{v}_n to denote n_{th} Fourier coefficient of expected momentum anisotropy in $\delta p/p$ defined in the lab frame. Here δp represents fluctuation in the momentum p of the final particles from the average momentum, in a given azimuthal angle bin.

We should clarify that in the conventional analysis, v_2 is directly related to the elliptical shape of the fireball, and normally one does not call it a fluctuation. However, in our language, the elliptic shape of the fireball itself is taken to represent a fluctuation (of large wavelength) from isotropic case. As our analysis is carried out in the Lab fixed frame, all shape fluctuations (including the elliptical ones) are treated uniformly by calculating different Fourier coefficients F_n .

Again we emphasize the most important difference between the conventional discussions of the elliptic flow and our analysis; here one does not try to determine any special reaction plane on event-by-event basis. A fixed coordinate system is used for calculating azimuthal anisotropies. This is why, as discussed in Sect.II and as is seen in the plots in ref.[1], averages of F_n s (and hence of \tilde{v}_n s) vanish when large number of events are included in the analysis. However, the root mean square values of F_n s, and hence of \tilde{v}_n s, are non-zero in general and contain non-trivial information. In fact, it is the same as the standard deviation for the distribution of F_n s since the average value of F_n s is zero. This is what is exactly done for the CMBR case also [5].

One important difference from CMBR, which may be of crucial importance in finding any non-trivial features in the plot of \tilde{v}_n^{rms} for RHICE, is the fact that for the CMBR case, for each l mode of the spherical harmonic, there are only $2l + 1$ independent measurements available, as there is only one CMBR sky to observe. For small l values this becomes dominant source of uncertainty, leading to the accuracy limited by the so called cosmic variance [5]. In contrast, for RHICE, each nucleus-nucleus collision (with same parameters like collision energy, centrality etc.) provides a new sample event. Also, in the absence of any special reflection symmetry here (which was present in the traditional elliptic flow analysis) all flow coefficients give non-zero contributions to \tilde{v}_n^{rms} , and the “sin” terms give same values as the “cos” terms. In the plots of \tilde{v}_n^{rms} below, we show the sum of these two contributions, i.e. square root of the sum of the squares of the “sin” term and the “cos” term

III. RESULTS FOR NON-CENTRAL COLLISIONS

We have generated events using HIJING and we present sample results for Au-Au collision at 200 GeV/A center of mass energy. In all the plots, the averages are taken over 10000 events, and the root mean square values \tilde{v}_n^{rms} of the flow Fourier coefficients are obtained from spatial F_n s simply by using proportionality factor of 0.2. The relation between the Fourier coefficients of the spatial anisotropy and resulting momentum anisotropy in our model can only be obtained using a full hydrodynamical simulation, with proper accounts of any surface tension, as well as factors such as horizon crossing etc. to properly account for the physics discussed here. In the absence of such a simulation, we make a strong assumption here that all Fourier coefficients for momentum anisotropy are related to the corresponding coefficients for spatial anisotropy by roughly the same proportionality factor, which we take to be 0.2 for definiteness. (As mentioned in ref.[1], this choice also gave reasonably good agreement with the results for \tilde{v}_2^{rms} in the literature for (almost) central events [4].) Although overall shape of the plot of \tilde{v}_n^{rms} will crucially depend on the values of these proportionality constants, and hence may change completely from what is shown here, the qualitative features such as the presence of peaks may remain unaffected. (Though, the peak positions may shift depending on these proportionality constants.) F_n s are calculated directly from the parton energy distribution at $t = 1$ fm for each event, within unit central rapidity window.

Fig.1 presents plots of \tilde{v}_n^{rms} for different values of impact parameters. Solid, dashed, and dotted plots correspond to impact parameter $b = 0, 5$ fm, and 8 fm, respectively with the spread in b taken to be 1 fm for non-zero b cases. The solid plot for central collisions shows monotonically decreasing values of \tilde{v}_n^{rms} . We emphasize that even here the plot has non-trivial structure compared to the case when partons are randomly distributed inside the nuclear volume with uniform probability, which yields a flat plot for corresponding \tilde{v}_n^{rms} . (Though, the rise of $b = 0$ plot for small n does not appear prominent here due to larger vertical scale of the plot.) Errors in these plots are very small.

Important thing to note is the prominent peak in non-central collisions for $b = 5$, and 8 fm at $n = 2$. The peak height is significantly larger for $b = 8$ fm. Important thing to realize is that this feature (which within our model simply represents elliptical distribution of partons in position space at the initial time) is present even when the \tilde{v}_n^{rms} have been calculated in a lab fixed reference frame. Average values of \tilde{v}_n for all values of impact parameters,

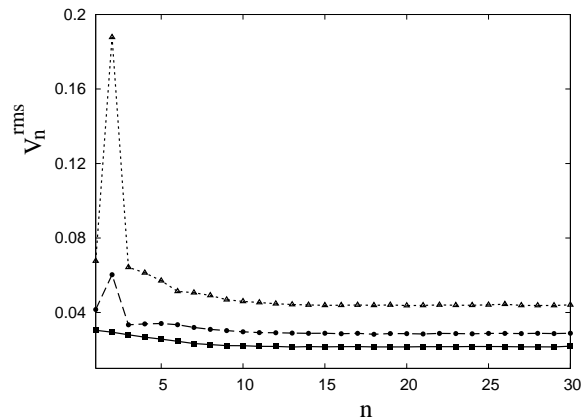


FIG. 1: These plots show smooth joining of the values of \tilde{v}_n^{rms} calculated from Fourier coefficients F_n s of the initial spatial anisotropy as discussed in text. Plots are obtained using 10000 events from HIJING. Solid, dashed, and dotted plots correspond to impact parameter $b = 0, 5$ fm, and 8 fm, respectively. Note the prominent peak at $n = 2$ for non-zero b cases.

calculated for large number of events, continue to be zero as shown in ref. [1] for the central collision case. This is expected from rotational symmetry in lab fixed frame. Larger overall values of \tilde{v}_n^{rms} for larger values of b are simply due to smaller number of initial partons leading to larger fluctuations. We mention that the solid plot in Fig.1 is given exactly for $b = 0$ to show the difference between zero and non-zero b cases. However, with experimental data, $b = 0$ will inevitably include events with small but non-zero values of b . Thus even for $b = 0$ case one should expect to observe a (small) peak at $n = 2$.

We have also calculated the root mean square values of the Fourier coefficients of the momentum anisotropy directly using the momenta of final particles from HIJING. These plots are all similar to each other for all values of the impact parameter b and hence similar to the central case $b = 0$ (apart from larger statistical fluctuations for larger values of b due to smaller number of partons as discussed above for Fig.1.) This is expected because, despite initial spatial anisotropy of parton production for non-central collisions, momentum distribution remains isotropic in the absence of any hydrodynamic evolution. We do not show these momentum plots here because such plots have been given in ref.[1] for the central collision case.

Fig.1 shows the strength of this technique of plotting root-mean-square values of flow coefficients in lab fixed coordinate frame as compared to the traditional analysis of elliptic flow. This technique is simple to implement (apart from the issue of non-flow correlations [7, 8], which one has to resolve in any case), allowing larger statistics to be generated. What one needs is predictions from hydrodynamics about \tilde{v}_n^{rms} calculated in lab fixed frame and then compare with data analyzed similarly. As the plots in Fig.1 show, the values of \tilde{v}_n^{rms} even for very large values of n continue to be significantly non-zero and with the possibility of sufficient statistics, one may be able to determine any important features in these plots.

In [1] we had argued that certain important aspects of inflationary density fluctuations, such as suppression of superhorizon modes and acoustic oscillations may also be present in these plots of \tilde{v}_n^{rms} in RHICE. Basic ideas can be stated as follows. Acoustic peaks in CMBR primarily result from the coherence and acoustic oscillations of the inflationary density fluctuations with coherence originating from the superhorizon nature of fluctuations, essentially freezing the fluctuations on superhorizon scales. This should be reasonably true for RHICE as the transverse velocity to begin with is expected to be zero and becomes non-zero only due to pressure gradients (which does not become fully effective on superhorizon scales). The oscillatory behavior for the fluctuations in the universe results from attractive forces of gravity and counter balancing forces from radiation pressure (with the coupling of baryons to the radiation). The oscillatory behavior of the fluctuations in RHICE is expected due to flow development with non-zero pressure gradients, at least for sufficiently small wavelength modes. These arguments suggest that some features like acoustic peaks may be present in the plots of \tilde{v}_n^{rms} for RHICE also. Further, modes with wavelengths larger than the acoustic horizon size H_s^{fr} at freezeout should be naturally suppressed as pressure gradients do not become fully effective on those scales to generate full flow anisotropy before freezeout occurs. This leads to the following suppression factor

$$(\tilde{v}_n)_{observed} = \frac{2H_s^{fr}}{\lambda} (\tilde{v}_n)_{max} \quad (8)$$

where $\lambda \sim 2\pi\bar{R}^{fr}/n$, ($n \geq 1$), is the measure of wavelength of the anisotropy corresponding to the n_{th} Fourier coefficient. Here \bar{R}^{fr} represents the transverse radius at the freezeout time τ_{fr} . Using the rough estimate of the

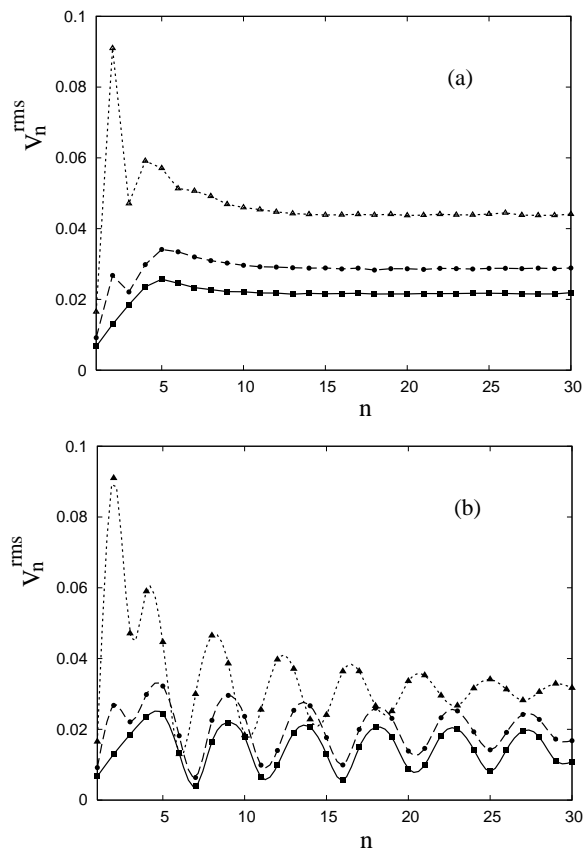


FIG. 2: These plots are obtained from the values of \tilde{v}_n^{rms} of the plots in Fig.1 by including (a) the suppression factor given in Eq.(8) for superhorizon modes, and (b) including acoustic oscillations as well. The plots here only show the modeling of the type of suppression factor and oscillations discussed in the text, which are superimposed on the plots in Fig.1.

rate of change of the transverse velocity to be about 0.1 fm^{-1} at the early stages at these energies [9], we can estimate $\bar{R}^{fr} \simeq \bar{R} + 0.05(\tau_{fr} - \tau_{eq})^2 = \bar{R}(1 + 0.05\bar{R}/c_s^2)$. Here $\bar{R} \equiv \bar{R}(\tau_{eq}) = c_s(\tau_{fr} - \tau_{eq})$. The largest wavelength λ_{max} of spatial anisotropy which will have chance to develop to its maximum hydrodynamic value is, therefore, $\lambda_{max} \simeq 2H_s^{fr} = 2c_s(\tau_{fr} - \tau_{eq}) = 2\bar{R}(\tau_{eq})$. This gives us the corresponding minimum value n_{min} of n below which flow coefficients should show suppression due to being superhorizon,

$$n_{min} = \pi \left(1 + \frac{0.05\bar{R}(\tau_{eq})}{c_s^2} \right) \quad (9)$$

The possibilities of the superhorizon suppression and acoustic oscillations lead to new peak structures in the plot of \tilde{v}_n^{rms} as was shown in [1] for central collisions. It is therefore important to know whether the peak in \tilde{v}_n^{rms} due to elliptic flow for non-central collisions (as in Fig.1) survives if these new features are also present, especially with the suppression of superhorizon modes at smaller n . For this purpose, we show in Fig.2, plots (for different values of impact parameter b as in Fig.1), when superhorizon suppression is included and when acoustic oscillations are also included in modeling the values of \tilde{v}_n^{rms} . It is clearly seen that the peak at $n = 2$ corresponding to the elliptic flow is present in all the plots and remains most prominent for $b = 8 \text{ fm}$.

Here we mention that recently Sorensen has proposed [10] a novel explanation of azimuthal correlations observed at the Relativistic Heavy-ion Collider (RHIC) at BNL in terms of the suppression of the superhorizon fluctuations discussed in [1]. One of the plots (Fig.4) in [10] (where suitable subtraction of v_2 has been made) shows possible suppression of values of the variance for small n , as predicted in [1].

We mention that we calculate \tilde{v}_n^{rms} by direct calculation of variances of the distributions of \tilde{v}_n (actually F_n s) in the laboratory fixed frame. Equivalently one can calculate \tilde{v}_n^{rms} by calculating the two-particle azimuthal correlation functions, as is done for the elliptic flow calculations. To extract elliptic flow coefficient from two-particle azimuthal correlations one has to separate non-flow contributions [7, 8]. Two particle azimuthal correlations, which are experimentally measured, contain contributions from non-flow effects such as jets, resonance decays, HBT correlations,

final state interactions etc. Various methods have been discussed to separate out the non-flow contributions to the azimuthal correlations [7, 8]. Our estimates of \tilde{v}_n^{rms} will also contain such non-flow contributions which have to be properly accounted for.

IV. p_T DEPENDENCE

In the conventional analysis of elliptic flow, v_2 has a non-trivial dependence on p_T of hadrons [11]. v_2 increases with p_T , saturates, and then decreases. Initial increase of v_2 with p_T is easily determined [12, 13, 14]. Large p_T behavior of flow is governed by viscous effects, parton energy loss, as well as by parton coalescence [11]. The same physics will be applicable in our model as well. For simplicity, we will follow the approach in ref. [12] where the linear increase of the elliptic flow v_2 with p_T is determined to be

$$v_2 = \frac{\alpha}{T}(p_T - vm_T) \quad (10)$$

where α characterizes the magnitude of elliptic flow, v is the flow velocity (see below) and $m_T = \sqrt{p_T^2 + m^2}$ is the transverse mass. We mention that this linear dependence of v_2 on p_T is expected for the intermediate range of p_T . The behavior for small p_T may be more non-trivial [14]. However, recall from Eq.(6) (and discussion in Sect.II) that in the context of our model, \tilde{v}_2^{rms} is simply given by the conventional v_2 , hence whatever be the dependence of v_2 on p_T , \tilde{v}_2^{rms} should show the same dependence. Still, it is useful to directly check the expected p_T dependence of \tilde{v}_2^{rms} in our model by adopting the analysis of v_2 in ref. [12] for our case. This is for two reasons. First, the relevance of random fluctuations needs to be assessed at different stages of the calculations to see the effects of event averaging and to see whether similar statements can be made about other flow coefficients. (For example, see the discussion following Eq.(12) below about the form of the fluid 4-velocity.) Secondly, the analysis for v_2 in ref. [12] is carried out to linear order in α . Since we calculate the root mean square values, we need to keep terms of order α^2 . Though, as we will see below, the α^2 term will turn out to be only relevant for v_4 and will not affect the analysis of \tilde{v}_2^{rms} .

We start by noting that the expression for v_2 in Eq.(10) corresponds to the conventional analysis with the determination of event plane. In our approach, the analysis is carried out in the lab fixed frame. For each non-central event the magnitude of the flow anisotropy will still be characterized by (say) the above equation. However, the maximum flow direction will now vary randomly from one event to another because the event plane is left undetermined. Thus, it looks reasonable to expect that \tilde{v}_2^{rms} should show the same dependence on p_T as v_2 in Eq.(10), as is indeed shown by Eq.(6). We will check this directly by adopting the analysis of v_2 in ref. [12] for our case for the estimation of \tilde{v}_2^{rms} in the lab fixed frame (and keeping terms of order α^2). Let us start with the transverse momentum distribution of emitted particles [12]

$$\frac{dN}{p_T dp_T dp_z d\phi} \equiv \rho(\phi) \propto \exp\left(\frac{-m_T u^0(\phi) + p_T u(\phi)}{T}\right) \quad (11)$$

Here, $u(\phi)$ is the space component of the fluid flow 4-velocity u_μ in ϕ direction, and $u^0(\phi)$ is the time component. For non-central collisions, the anisotropic flow can be parameterized as

$$u(\phi) = u + 2\alpha \cos 2(\phi - \psi) \quad (12)$$

Here u is the angular average of maximum fluid 4-velocity, and $\alpha > 0$ characterizes the magnitude of elliptic flow. Note, that we have introduced here the angle ψ characterizing the orientation of the event plane in the lab frame so that the angle ϕ is measured in the lab frame. Also, it is important to realize that here we are only characterizing elliptic flow anisotropy of the fluid, without worrying about the presence of general fluctuations. The justification for this is that, as can be seen from Fig.1, for non-central collisions in our method it is only \tilde{v}_2^{rms} which has a significantly larger value than the values of \tilde{v}_n^{rms} for other n . Thus, the presence of general fluctuations (as accounted for in Fig.1) will play an important role in determination of these other values of \tilde{v}_n^{rms} even for non-central collisions. In contrast, for \tilde{v}_2^{rms} the elliptic anisotropy resulting from non-central collision seems to play dominant role over the random fluctuations. Hence the parametrization of Eq.(12) may capture important aspects of the dependence of \tilde{v}_2^{rms} on p_T etc.

We are interested in calculating the root mean square value (instead of v_2 as in ref. [12]). Thus, we expand $u^0(\phi) = \sqrt{u(\phi)^2 + 1}$ to second order in α , and get (with $v = u/u^0$),

$$u^0(\phi) = u^0 + 2\alpha v \cos 2(\phi - \psi) + \frac{2\alpha^2}{(u^0)^3} \cos^2 2(\phi - \psi) \quad (13)$$

Using this equation, and Eq.(11), we get particle transverse momentum distribution as

$$\rho_\psi(\phi) = A[1 + 2\alpha \cos 2(\phi - \psi) \frac{(p_T - vm_T)}{T} + \alpha^2(1 + \cos 4(\phi - \psi))(\frac{(p_T - vm_T)^2}{T^2} - \frac{m_T}{T(u^0)^3})] \quad (14)$$

where A is independent of ϕ, ψ . We see that this equation is in the same form as Eq.(2). It is important to note here that the α^2 term here only comes for v_4 (requiring higher powers of α for the calculation of \tilde{v}_4^{rms}) and v_2 remains linear in α .

Following the discussion in Sect.II following Eq.(2), and using Eq.(6), we immediately see that

$$\tilde{v}_2^{rms} = \frac{\alpha}{T}(p_T - vm_T) \quad (15)$$

Which is the same dependence on p_T as in Eq.(10) for the conventional analysis of v_2 using event plane determination.

We again emphasize that in our picture, the randomness in the orientation of the event plane w.r.t. the lab fixed frame is easy to model by introducing angle ψ . The other intrinsic sources of fluctuations will also contribute to \tilde{v}_2^{rms} in our method, but as shown in Fig.1, their contributions appear to remain small (as seen by the plot for $b = 0$). (Note again, overall larger scale of plots of \tilde{v}_n^{rms} for larger values of b is primarily due to smaller number of particles leading to larger statistical fluctuations.) As we had discussed earlier, \tilde{v}_n^{rms} for $n \neq 2$ may be dominated by these intrinsic sources of fluctuations. If the contribution of such fluctuations remains sub dominant, then our results show that direct determination of v_2 , in particular its p_T dependence ([14]) is possible by measuring \tilde{v}_2^{rms} in lab fixed frame completely avoiding the determination of event plane.

V. DETECTOR ACCEPTANCE

One of the main advantages of using the techniques proposed here is that it makes it much easier to extract the information about flow without any need for event plane determination. Thus large amount of data can be analyzed improving accuracy. It then becomes important to address the issue of being able to incorporate data with varying azimuthal acceptance, as has been emphasized for the conventional flow analysis. Several methods have been proposed for accounting for azimuthal dependence of detector acceptance in the conventional flow analysis [8, 15]. These can be suitably adopted to the method proposed here. As mentioned above, due to fixed lab frame being used for analysis, the average values of all flow coefficients will be zero here due to azimuthal symmetry. Clearly, this will no longer be true in the presence of azimuthal anisotropy in the detector acceptance. For example, let $A(\phi)$ be the acceptance function characterizing the probability that a hadron is detected at azimuthal angle ϕ , with $A(\phi)$ being normalized as [8, 15]

$$\int_{-\pi}^{\pi} A(\phi) d\phi = 2\pi \quad (16)$$

In the lab fixed frame, the values of \tilde{v}_n in our method may be calculated from Eq.(3) (Sect.II). Note that for anisotropic detector acceptance there is an implicit factor of $A(\phi)$ in the integrand in Eq.(3). One can then directly calculate the event average value $\overline{\tilde{v}_n}$ of these flow coefficients \tilde{v}_n , by averaging \tilde{v}_n over a large number of events (of similar type, e.g. centrality etc.). The actual value of $\overline{\tilde{v}_n}$, for non-central collisions, is determined by the following expression

$$\overline{\tilde{v}_n} = \frac{1}{2\pi} \int_{-\pi}^{\pi} \left(\frac{1}{2\pi} \int_{-\pi}^{\pi} A(\phi) \rho_\psi(\phi) e^{-in\phi} d\phi \right) d\psi \quad (17)$$

Here, ψ denotes the orientation of the event plane in the lab fixed frame (see, Eq.(4) in Sect.II), which varies from event to event. We have made here explicit the acceptance function $A(\phi)$ in the above expression. (For simplicity

we assume that $A(\phi)$ does not depend on rapidity, p_T etc.). For ideal detector with uniform acceptance $A(\phi) = 1$ and by changing the order of $d\phi$ and $d\psi$ integrations one can easily see that $\overline{v_n} = 0$ as discussed in Sect.II (following Eq.(4)). However, for anisotropic acceptance, with $A(\phi) \neq 1$, $\overline{v_n}$ need not be zero. In fact, apart from a normalization (relating to angular average of ρ), $\overline{v_n}$ gives the Fourier coefficients for the series expansion of the function $A(\phi)$, thus allowing us to determine the acceptance function $A(\phi)$ directly from experimental data [8, 15].

For the simple case when $A(\phi)$ is non-zero for every ϕ , one can directly use $A(\phi)$, determined from $\overline{v_n}$ as explained above, to compensate for the effect of anisotropic detector acceptance by including additional factor of $1/A(\phi)$ in the integrand of Eq.(3) for calculation of \tilde{v}_n .

$$\tilde{v}_n = \frac{1}{2\pi} \int_{-\pi}^{\pi} \frac{\rho_\psi(\phi)}{A(\phi)} e^{-in\phi} d\phi \quad (18)$$

With this modification, Eq.(17) shows that the event average value $\overline{\tilde{v}_n}$ will again be zero, just as for the case of isotropic detector acceptance. The above Eq.(18) can then be used to determine the values of \tilde{v}_n^{rms} as discussed in earlier sections.

However, for more general case, e.g. for incomplete detector coverage, where $A(\phi) = 0$ for a range of ϕ the above simple method does not help. For such cases one can adopt the techniques discussed in [8, 15] for the present case. Though, due to the important role played by the event plane determination, these techniques need to be suitably adopted for our case where a fixed lab frame is used for the analysis. In fact, it is more helpful to directly adopt the techniques used for CMBR case where one uses a fixed lab frame (say, galactic coordinates) for writing down temperature anisotropies in the sky in terms of spherical harmonics. For CMBR analysis also one needs to compensate for the effects of partial coverage of the sky. This happens either due to limited coverage of the sky by the detector, or due to galactic foreground as for WMAP [16]. Adopting that approach for our case, we start with the experimentally determined flow coefficients v_n for each event (which, following [16] we call *pseudo* flow coefficients).

$$v_n = \frac{1}{2\pi} \int_{-\pi}^{\pi} e^{-in\phi} A(\phi) \rho_\psi(\phi) d\phi \quad (19)$$

where, now, $A(\phi)$ may be zero for a range of ϕ values. Using Fourier coefficients a_m for the acceptance function $A(\phi)$, we get,

$$v_n = \frac{1}{2\pi} \int_{-\pi}^{\pi} \sum_m a_m e^{-i(n-m)\phi} \rho_\psi(\phi) d\phi = \sum_l a_{(n-l)} \tilde{v}_l \quad (20)$$

where \tilde{v}_l is the true flow coefficient (defined with respect to the lab fixed frame). The above equation shows the mode-mode coupling of flow coefficients resulting from incomplete detector coverage [8, 15, 16]. For an approximate determination of \tilde{v}_l we can use appropriate truncation of the above matrix equation to a finite set of linear equations and solve for \tilde{v}_l . This analysis can be done for each event, and with the values of \tilde{v}_l thus determined one can directly get the estimate of the true variance \tilde{v}_n^{rms} for a set of events.

VI. CONCLUSIONS

In summary we emphasize the important lessons from CMBR analysis techniques. We have argued that important information about initial anisotropies of the system and their evolution in relativistic heavy-ion collisions can be obtained by plotting the root mean square values of the Fourier coefficients \tilde{v}_n^{rms} of the anisotropies in the fluctuations $\delta p/p$ of the particle momenta, calculated in a fixed laboratory frame, starting from $n = 1$ upto large values of $n \simeq 30$. (which corresponds to $\lambda \sim 1$ fm). Note that $n = 30$ almost corresponds to wavelength of fluctuation λ at the surface of the region, at τ_{fr} , being of order 1 fm. Fluctuations with wavelengths smaller than 1 fm presumably cannot be treated within hydrodynamical framework, so we restrict attention within this range of n . One will expect that beyond a critical value of n the nature of the curve should change in some qualitative manner indicating breakdown of underlying hydrodynamical description for smaller modes. The wavelength corresponding to that critical value of n will determine the smallest scale below which hydrodynamical description is not valid. The plot of \tilde{v}_n^{rms} for n larger than this critical value will probe fluctuations in parton density at even smaller length scales and may provide a bridge with the perturbative regime.

For non-central collisions our technique provides a direct method to probe elliptic flow by determining \tilde{v}_2^{rms} in lab fixed frame. If random fluctuations do not dominate then our results show that \tilde{v}_n^{rms} can directly probe $|v_n|$ for $n \neq 2$

also. This may be important for collisions of deformed nuclei. It is important to appreciate that a plot of \tilde{v}_n^{rms} tells us about the statistical nature of fluctuations and anisotropies of the initial plasma region (just as in the CMBR case), hence it will always have valuable information irrespective of its shape (e.g. a flat curve). Hydrodynamical simulations, with proper incorporation of such fluctuations can be used to predict directly the values of \tilde{v}_n^{rms} whose comparison with data will constrain/determine various physical inputs such as equation of state, viscosity etc. Further, in analogy with CMBR analysis, one can determine higher moments of momentum anisotropies (again in lab fixed frame, as we have discussed above) probing detailed nature of initial fluctuations, e.g. non-Gaussianity etc. We hope to present a more detailed analysis of such issues in a future work. We also intend to explore various aspects of *horizon entering* of density fluctuations which can be probed under laboratory conditions using RHICE. This may help in bringing at least some aspects of inflationary physics (e.g. causal aspects, excluding those features which relate directly to gravity) of the universe under some experimental control.

Acknowledgments

We are very grateful to Raju Venugopalan, Rajeev Bhalerao, and Sergei Voloshin for very useful comments and suggestions. We also thank Sanatan Digal, Abhishek Atreya and Anjishnu Sarkar for useful comments.

-
- [1] A. P. Mishra, R. K. Mohapatra, P. S. Saumia, and A. M. Srivastava, Phys. Rev. **C 77**, 064902 (2008).
 - [2] M. Gyulassy, D. H. Rischke, and B. Zhang, Nucl. Phys. **A 613**, 397 (1997).
 - [3] J.-Y. Ollitrault, Phys. Rev. **D 46**, 229 (1992); S. Voloshin and Y. Zhang, Z. Physik **C70**, 665 (1996); S.A. Volosin, A.M. Poskanzer, and R. Snellings, arXiv:0809.2949.
 - [4] B. M. Tavares, H. J. Drescher, and T. Kodama, Braz. J. Phys. **37**, 41 (2007); P. Sorensen (for the STAR collaboration), J. Phys. **G 34**, S897 (2007); S. Manly et al. (for PHOBOS collaboration), nucl-ex/0702029; H. Sorge, Phys. Rev. Lett. **82**, 2048 (1999).
 - [5] S. Dodelson, "Modern Cosmology", (Academic Press, California, 2003).
 - [6] X.N. Wang and M. Gyulassy, Phys. Rev. **D 44**, 3501 (1991); Comput. Phys. Commun. **83**, 307 (1994).
 - [7] N. Borghini and J.-Y. Ollitrault, Phys. Rev. **C 70**, 064905 (2004); X. Dong, S. Esumi, P. Sorensen, N.Xu, and Z. Xu, Phys. Lett. **B 597**, 328 (2004)
 - [8] N. Borghini, P. M. Dinh, and J.-Y. Ollitrault, Phys. Rev. **C 64**, 054901 (2001).
 - [9] P.F. Kolb, J. Sollfrank, and U. Heinz, Phys. Rev. **C 62**, 054909 (2000).
 - [10] P. Sorensen, Proc. 24th Winter Workshop on Nuclear Dynamics, 2008, arXiv:0808.0503.
 - [11] M. Gyulassy, I. Vitev, X.N. Wang, Phys.Rev.Lett. **86**, 2537 (2001); Y. Bai (for STAR collaboration), J.Phys. **G34**, S903 (2007); B.I. Abelev et al. (for STAR Collaboration), Phys.Rev. **C77**, 054901 (2008).
 - [12] J.-Y. Ollitrault, Eur. J. Phys. **29**, 275 (2008).
 - [13] N. Borghini, and J.-Y. Ollitrault, Phys. Lett. **B 642**, 227 (2006).
 - [14] P. Huovinen, P.F. Kolb, U. Heinz, P.V. Ruuskanen, and S.A. Voloshin, Physy. Lett. **503**, 58 (2001).
 - [15] I. Selyuzhenkov and S. Voloshin, Phys. Rev. **C 77**, 034904 (2008); R. S. Bhalerao, N. Borghini, and J.-Y. Ollitrault, Nucl. Phys. **A 727**, 373 (2003).
 - [16] E. Hivon, et al. Astrophys. J. **567**,2 (2002).